Enhanced Spatial Network Method for the Analysis of Open Microstrip Discontinuities

Dragos M. Bica, *Student Member, IEEE,* and Benjamin Beker, *Senior Member, IEEE*

***Abstract*—In this paper, a new technique is presented for the numerical analysis of open boundary three-dimensional (3-D) vias embedded in multilayered strata. This approach is based on an enhanced spatial network method (SNM) algorithm, and leads to speed-up factors of 10–12 over the standard SNM implementation. Absorbing boundary conditions, based on the perfect matching layer (PML) concept, are implemented for open boundary truncation. Unlike the standard PML's, the proposed absorbing boundary conditions (ABC's) do not require introduction of additional variables.**

***Index Terms*—Absorbing boundary conditions, finite differencing, microstrip discontinuities, time-domain modeling.**

I. Introduction

THE ADVANCES in microwave integrated circuit (MIC) technology and the increased need for higher circuit densities have resulted in greater proliferation of MIC discontinuities. Their effects on circuits, which contain multiple signal layers, have to be correctly predicted, especially in high-frequency (HF) designs. One of the most common discontinuities is a via, which provides an electrical path between signal lines on different layers.

The characterization of three-dimensional (3–D) microstrip discontinuities has been previously confined to two main approaches: the semianalytical formulations of specific problems or to the purely numerical general-purpose algorithms. Both methodologies are capable of yielding results for the S-parameters in the frequency domain. The semianalytic methods are a blend of the method of moments (MoM) with the spectral-domain approach, which lead, for example, to the so-called spatial-domain method [1]. This approach has been demonstrated in the study of 3-D problems, such as vias embedded in multilayered dielectric strata. At higher frequencies (for open structures) the surface waves and radiation losses can no longer be ignored. In this case, to correctly describe the current along a vertical post between two microstrips, such as the via, pulse functions were used in the MoM formulation of the scattering problem [2].

Presently, for the purely general-purpose numerical techniques for the modeling of such discontinuities, the best-known methods are the finite-difference time-domain (FDTD) and transmission-line matrix (TLM) methods. Both of these techniques have been used to characterize the electrical properties of 3-D microstrip discontinuities. TLM, in its frequency domain form, has been employed in the computation of the S-parameters for transmission line interconnects, such as vias and air bridges [3]. FDTD has also been utilized in the study of vias, among other irregular geometries [4]. The time-domain results of FDTD are usually transformed into the frequency domain using the fast Fourier transform (FFT) to obtain the S-parameters.

In order to analyze open boundary problems, all differential-equation-based methods need to be linked to absorbing boundary condition (ABC) algorithms. Thus far, the most popular types of ABC's have included factoring of the one-way equations, or introducing artificial lossy layers into part of the computational domain, which is then truncated by a metallic wall. The latter method is referred to as the perfect matching layer (PML) approach, and to date has been shown to lead to the lowest artificial reflection coefficients when used in conjunction with FDTD.

In this paper, the new enhanced spatial network (ESN) method algorithm, which is derived from the conventional SNM [5], is used in conjunction with PML's for the electrical characterization of vias embedded in multilayer structures within open MIC environments. Compared to the SNM, the ESN is about 10–12 times faster and requires about half the memory of previous SNM implementations. The PML's are specialized for the ESN and do not require the introduction of additional variables. They are applied for the first time to the ESN algorithm and they yield reflection coefficients ranging from -41 to -26 dB for normal wave incidence, depending on the number of dielectric layers contained in the substrate.

II. Theory

A. Formulation of ESN

The basics of the SNM algorithm have been described extensively in [5], and, therefore, will not be repeated. However, to point out where the ESN departs from the standard SNM, the governing equations of the SNM are restated for completeness. Similar notations, as well as current and voltage definitions (in terms of electromagnetic (EM) fields), which were introduced in [5], will be used in the following discussion.

For the electric (E_x) node $v_{ex}(i,j,k)$ (Fig. 1), the nodal equation can be derived assuming that from the adjacent magnetic nodes at timestep t, waves are launched toward the central node, reaching it at timestep $t+1$. For the waves

Manuscript received March 12, 1996; revised February 28, 1997. This work was supported by the U.S. Army Research Office under Grant DAAL03-92-G-0275.

The authors are with the Department of Electrical and Computer Engineering, University of South Carolina, Columbia, SC 29208 USA.

Publisher Item Identifier S 0018-9480(97)03912-4.

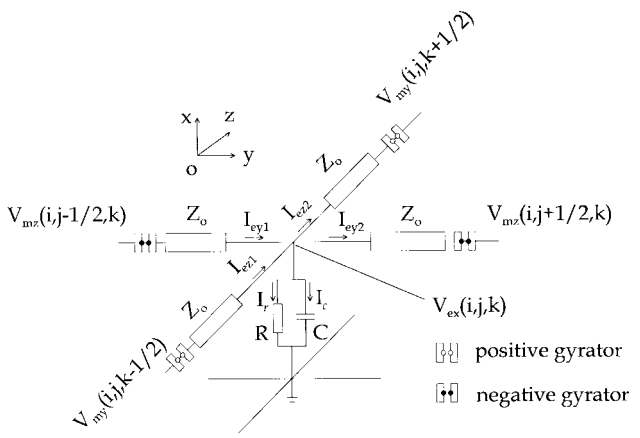

Fig. 1. V_{ex} electric node specific to the SNM algorithm.

launched from the surrounding nodes ($v_{my}(i,j,k\pm 1/2)$ and $v_{mz}(i,j\pm 1/2,k)$), the wave equations are

$$\begin{aligned} &v_{ex}^{t+1}(i,j,k)\pm Z_0\cdot i_{ez1;2}^{t+1}(i,j,k)\\ &\quad= i_{mz2;1}^{t}(i,j,k\mp 1/2)\pm \mathrm{Z}_0\cdot v_{my}^{t}(i,j,k\mp 1/2)\\ &\quad= \Psi_{m1;2}^{t}\\ &v_{ex}^{t+1}(i,j,k)\pm Z_0\cdot i_{ey1;2}^{t+1}(i,j,k)\\ &\quad= -\big(i_{my2;1}^{t}(i,j\mp 1/2,k)\pm \mathrm{Z}_0\cdot v_{mz}^{t}(i,j\mp 1/2,k)\big)\\ &\quad= \Psi_{3;4}^{t} \end{aligned} \tag{1}$$

where $Z_0=\sqrt{\mu_0/\varepsilon_0}$ is the characteristic impedance of the transmission lines. In addition to the currents entering the $v_{ex}(i,j,k)$ node via the transmission lines, there are also currents through the resistor and capacitor connected to the node. The final nodal equation for $v_{ex}(i,j,k)$ is obtained by enforcing Kirchoff's current law, which yields (2a), as shown at the bottom of the page, where

$$R_c(i,j,k)=\frac{4\cdot\Delta t\cdot c_0}{\varepsilon_0\cdot(\varepsilon_r(i,j,k)-1)\cdot\Delta x} \tag{2b}$$

$$R(i,j,k)=G^{-1}(i,j,k)=\frac{2\cdot\Delta x}{\sigma(i,j,k)}. \tag{2c}$$

The $\Psi_{mk}^{t}(i,j,k)$ terms, given by the right-hand side (RHS) of (1) account for the waves propagating toward the v_{ex} node on the four transmission lines surrounding it. Ψ_c is associated with the flow of current through the capacitor and is given by

$$\Psi_c^t(i,j,k)=V_{ex}^t(i,j,k)+R_c(i,j,k)\cdot I_{\mathrm{cex}}^t(i,j,k). \tag{3}$$

According to [5], the ratio $\bar{v}=\Delta x/(c_0\cdot\Delta t)$, which is interpreted as the normalized velocity of the algorithm, should be equal to 4.0—this limit being imposed by the definition of R_c in (2b). Similar equations can also be obtained for voltages at the magnetic nodes and in conjunction with (2a), can be used to solve the boundary value problem, as described in [5].

Reduction of the SNM algorithm begins with modifications to (1) by recasting them in terms of normalized voltages and currents ($V_{mq}=v_{mq}\cdot\sqrt{\mu_0}$, $V_{eq}=v_{eq}\cdot\sqrt{\varepsilon_0}$, $I_{mq}=i_{mq}\cdot\sqrt{\varepsilon_0}$, and $I_{eq}=i_{eq}\cdot\sqrt{\mu_0}$, where $q=x,y,z$). To make an explicit distinction between the electric and magnetic variables, the $\Psi_{mk}^{t}(i,j,k)$ terms are replaced with voltages and currents using (1) and the normalizations stated above. This leads to (4), as shown at the bottom of the page, where the following notation has been used:

$$\begin{aligned} V_{m\mathrm{TOT}x}^t=&V_{mz}^t(i,j+1/2,k)-V_{mz}^t(i,j-1/2,k)\\ &-V_{my}^t(i,j,k+1/2)+V_{my}^t(i,j,k-1/2) \end{aligned} \tag{5}$$

$$\begin{aligned} I_{m\mathrm{TOT}x}^t=&I_{mz1}^t(i,j,k+1/2)-I_{mz2}^t(i,j,k-1/2)\\ &-I_{my1}^t(i,j+1/2,k)-I_{my2}^t(i,j-1/2,k) \end{aligned} \tag{6}$$

$$g_{\mathrm{cex}}(i,j,k)=Z_0/R_{\mathrm{c}}(i,j,k)$$

$$g_{cx}(i,j,k)=Z_0/R(i,j,k) \tag{7}$$

and where I_{cex} is the current through the capacitor (Fig. 1).

To simplify the algorithm for the same electric node $V_{ex}(i,j,k)$, the currents denoted by $I_{m\mathrm{TOT}x}^t$ in (4) must be expressed in terms of electric and magnetic voltages only. Each of the currents comprising $I_{m\mathrm{TOT}x}^t$ is derived from nodal equations written for the magnetic nodes surrounding the electric node $V_{ex}(i,j,k)$

$$\begin{aligned} &I_{mz1;2}^t(i,j,k\pm 1/2)\\ &\quad=\mp V_{my}^t(i,j,k\pm 1/2)\pm I_{ez2;1}^{t-1}(i,j,k)+V_{ex}^{t-1}(i,j,k)\\ &I_{my1;2}^t(i,j\pm 1/2,k)\\ &\quad=\mp V_{mz}^t(i,j\pm 1/2,k)\mp I_{ey2;1}^{t-1}(i,j,k)-V_{ex}^{t-1}(i,j,k) \end{aligned} \tag{8}$$

allowing for $I_{m\mathrm{TOT}x}^t$ to be written as a function of $V_{ex}(i,j,k)$ and the surrounding magnetic voltages

$$\begin{aligned} I_{m\mathrm{TOT}x}^t=&\big(-V_{my}^t(i,j,k+1/2)+V_{my}^t(i,j,k-1/2)\\ &+V_{mz}^t(i,j+1/2,k)-V_{mz}^t(i,j-1/2,k)\big)\\ &+\big(I_{ez2}^{t-1}(i,j,k)-I_{ez1}^{t-1}(i,j,k)\\ &+I_{ey2}^{t-1}(i,j,k)-I_{ey2}^{t-1}(i,j,k)\big)+4V_{ex}^{t-1}(i,j,k). \end{aligned} \tag{9}$$

$$v_{ex}^{t+1}(i,j,k)=\frac{R_c(i,j,k)\cdot\big(\Psi_{m1}^t+\Psi_{m2}^t+\Psi_{m3}^t+\Psi_{m4}^t\big)(i,j,k)+Z_0\cdot\Psi_c^t(i,j,k)}{Z_0+R_c(i,j,k)\cdot(4+Z_0\cdot 4\cdot G(i,j,k))} \tag{2a}$$

$$V_{ex}^{t+1}(i,j,k)=\frac{I_{m\mathrm{TOT}x}^t+V_{m\mathrm{TOT}x}^t+g_{\mathrm{cex}}(i,j,k)\cdot V_{ex}^t(i,j,k)+I_{\mathrm{cex}}^t(i,j,k)}{4+g_{\mathrm{cex}}(i,j,k)+g_{cx}(i,j,k)} \tag{4}$$

Application of Kirchoff's current law in (9) for the currents at time $t-1$, and the usage of the result in (4), leads to the following finite-difference expression for $V_{ex}(i,j,k)$:

$$\begin{aligned} V_{ex}^{t+1}(i,j,k) &= \big((4-g_{cx}(i,j,k))\cdot V_{ex}^{t-1}(i,j,k) \\ &\quad + g_{\text{cex}}(i,j,k)\cdot V_{ex}^{t}(i,j,k) \\ &\quad + 2\cdot\big(-V_{mz}^{t}(i,j-1/2,k)+V_{mz}^{t}(i,j+1/2,k) \\ &\quad + V_{my}^{t}(i,j,k-1/2)-V_{my}^{t}(i,j,k+1/2)\big) \\ &\quad + I_{\text{cex}}^{t}(i,j,k)-I_{\text{cex}}^{t-1}(i,j,k)\big) \\ &\quad /(4+g_{cx}(i,j,k)+g_{\text{cex}}(i,j,k)). \end{aligned} \tag{10}$$

The above expression still contains a restrictive artifact from the SNM, namely, the normalized algorithm velocity $\overline{v}=\Delta x/(c_0\cdot\Delta t)=4.0$. To generalize this algorithm for any normalized velocity, the 4.0's are replaced with $\overline{v}$, and $g_{\text{cex}}(i,j,k)$ is redefined as $g_{\text{cex}}(i,j,k)=\overline{v}\cdot(\varepsilon_r(i,j,k)-1)$. As a result, the restriction on $\overline{v}$ can be removed and the stability of the algorithm can be analyzed for a whole range of new values of the normalized velocity.

With the generalizations mentioned above, (10) represents a new finite-difference scheme for updating V_{ex} (or E_x). It is equivalent to the SNM scheme, which uses central differences for the space and time derivatives. Unlike the SNM, the new algorithm employs only 12 variables for each unit cell. In addition, the proposed scheme is no longer restricted to a predefined normalized velocity, which was removed by redefining terms related to the dielectric (i.e., g_{cex}). It should be added that analogous expressions can also be derived for the remaining components of the EM fields and used together with (10) to solve the field problem.

Comparison of the standard SNM algorithm and the proposed ESN reveals that the SNM needs one voltage and five associated currents for each of the six nodes in a unit cell, adding up to a total of 36 variables per unit cell. The ESN reduces the number of variables per unit cell from 36 to 12, utilizing only one voltage and one current for each node. In addition to saving computer memory, this approach also reduces the number of computer operations per unit cell from six assignments, twenty additions, four multiplications and one division to two assignments, ten additions, four multiplications, and one division.

As a slight point of departure, it is also informative to add that further reduction in the number of variables per unit cell can be achieved. This is done by replacing the remaining capacitor currents in (10) with expressions containing electric voltages only. Applying a central finite-difference approximation to the v–i characteristic of the capacitor $i=C\cdot dV/dt$, allows for I_{cex} to be recursively defined as follows:

$$\begin{aligned} I_{\text{cex}}^{t}(i,j,k) &= g_{\text{cex}}(i,j,k)\cdot\big(V_{ex}^{t}(i,j,k)-V_{ex}^{t-1}(i,j,k)\big) \\ &\quad - I_{\text{cex}}^{t-1}(i,j,k). \end{aligned} \tag{11}$$

The resulting algorithm, which is obtained by repeatedly using (11) in the generalized form of (10), is shown below:

$$\begin{aligned} V_{ex}^{t+1}(i,j,k) &= \big((\overline{v}-g_{cx}(i,j,k))\cdot V_{ex}^{t-1}(i,j,k) \\ &\quad + g_{\text{cex}}(i,j,k)\cdot V_{ex}^{t}(i,j,k) \\ &\quad + 2\cdot\big(-V_{mz}^{t}(i,j-1/2,k)+V_{mz}^{t}(i,j+1/2,k) \\ &\quad V_{my}^{t}(i,j,k-1/2)-V_{my}^{t}(i,j,k+1/2)\big) \\ &\quad + g_{\text{cex}}(i,j,k)\cdot\big(V_{ex}^{t}(i,j,k)-2\cdot V_{ex}^{t-1}(i,j,k)+\cdots \\ &\quad + (-1)^{t}\cdot 2\cdot V_{ex}^{2}(i,j,k)+(-1)^{t+1}\cdot V_{ex}^{1}(i,j,k)\big)\big) \\ &\quad /\big(\overline{v}+g_{cx}(i,j,k)+g_{\text{cex}}(i,j,k)\big). \end{aligned} \tag{12}$$

Irrespective of the added benefits in further reducing the number of unknowns, the finite-difference scheme presented in (12) is impractical, and hence, was not used. It needs for the time history of every variable to be stored from time $t=0$ up to the present timestep.

B. Implementation of PML's for Open Boundaries

PML's were first proposed in [7] for two-dimensional (2-D) problems and later extended to 3-D problems in [8]. When used in FDTD, this technique doubles the number of variables at each node within the PML layer, to achieve independent attenuation of the field variables. The attenuation is accomplished by subjecting the material parameters within the PML layers to the following relationship:

$$\frac{\sigma_{x1}^{e}}{\varepsilon_1}=\frac{\sigma_{x2}^{e}}{\varepsilon_2}=\frac{\sigma_{x}^{m}}{\mu_0} \tag{13}$$

and using the regular FDTD algorithm to update the field components. This implementation of PML's has several drawbacks. First, it increases the computational volume and the number of unknowns. Secondly, it alters the stability of the main finite-difference algorithm, thus requiring a smaller $\Delta t/\Delta x$ ratio, which leads to longer computation times.

Thus far, only FDTD specific PML's have been implemented in the solution of guided-wave problems. The direct use of PML's, with splitting of field variables, as described in [8], was found to trigger numerical instabilities in the ESN. To overcome this, a modified form of the PML algorithm was implemented, based on the finite-differencing scheme of ESN.

It should be added that since Higdon ABC's have small reflections at grazing incidence, and do not require additional variables, they were used on all sidewalls of the lattice. At boundaries normal to the direction of propagation, however, the ESN-specific PML's were used, assuming that the basic mode of propagation is quasi-TEM.

As can be seen from (2) and (10), both the SNM and ESN contain expressions for the losses (terms G and g_{cx}, respectively). This suggests that sufficient attenuation of the fields within the PML layers [whose parameters are subjected to (13)] could be achieved without splitting the variables. Initial use of (10), with PML layers added to the ESN lattice, for attenuating the transverse components of the fields,

produced reflections as high as those due to Higdon ABC's for normal incidence (−23 dB). However, these reflections are not due to the lattice truncation boundary, but are attributed to the interface of the first PML layer. Further numerical investigation revealed that the regular ESN algorithm within the PML space exhibits near exponential decay. As a result, when a sufficient number of PML layers (16 layers) was used, the reflections from lattice boundaries became negligible.

Since the greatest source of reflections was found to be the conductivity of the first PML layer, its effect within the PML space had to be de-emphasized. This was accomplished (after an extensive numerical study) by neglecting the lossy terms in the denominator of (10), while still retaining the nearly exponential decay of the wave along the direction of propagation. As a result, the modified form of the ESN algorithm within the PML layers is given by

$$\begin{aligned} V_{ex}^{t+1}(i,j,k) &= \big((\bar{v} - g_{cx}(i,j,k)) \cdot V_{ex}^{t-1}(i,j,k) \\ &\quad + g_{\text{cex}}(i,j,k) \cdot V_{ex}^{t}(i,j,k) \\ &\quad + 2 \cdot \big(-V_{mz}^{t}(i,j-1/2,k) + V_{mz}^{t}(i,j+1/2,k) \\ &\quad + V_{my}^{t}(i,j,k-1/2) - V_{my}^{t}(i,j,k+1/2)\big) \\ &\quad + I_{\text{cex}}^{t}(i,j,k) - I_{\text{cex}}^{t-1}(i,j,k)\big)/(\bar{v} + g_{\text{cex}}(i,j,k)). \end{aligned} \tag{14}$$

The decay of the wave along the direction of propagation, which is built in (14), is less steep than that reported for FDTD PML's. This requires a thicker absorbing wall (24 cells as opposed to eight), but eliminates the use of additional variables, without causing significant reflections or instabilities. Compared to the Higdon ABC's, the ESN-specific PML's do not require a larger computational volume and lead to better performance (−23 dB versus −34 dB). The results of the above-proposed boundary truncation are presented in the next section.

III. Numerical Results and Conclusion

In order to assess the performance of the new ESN algorithm, multilayered discontinuities within open boundary environments were studied and the results were compared to previously published data. A via connecting signal lines on different layers of the dielectric, which is isolated by a ground plane, are shown in Fig. 2. The aim of the study was to obtain the S-parameters in the frequency domain. The standard approach for time-domain methods is to excite the structure with a Gaussian pulse and to store the incident, transmitted, and reflected waveforms. The S-parameters are subsequently obtained with the help of fast Fourier transform (FFT). This methodology is correct as long as both the physical dispersion of the structure and that of the numerical algorithm are low, and the reflections from the ABC's can be neglected.

The numerical dispersion of the ESN algorithm was analyzed for a uniform microstrip ($w = 0.9$ mm, $h = 0.9$ mm, and $\varepsilon_r = 2.2$), shown in Fig. 3, for a frequency range of 5–12 GHz. The computed phase velocity for each frequency point was normalized with respect to the phase velocity at 10 GHz. The physical dispersion of this microstrip is small, as can be shown from simple calculations using empirical results [13]. All the slight variations of the phase velocity reported in Fig. 3 are mainly attributed to the numerical dispersion of the ESN algorithm.

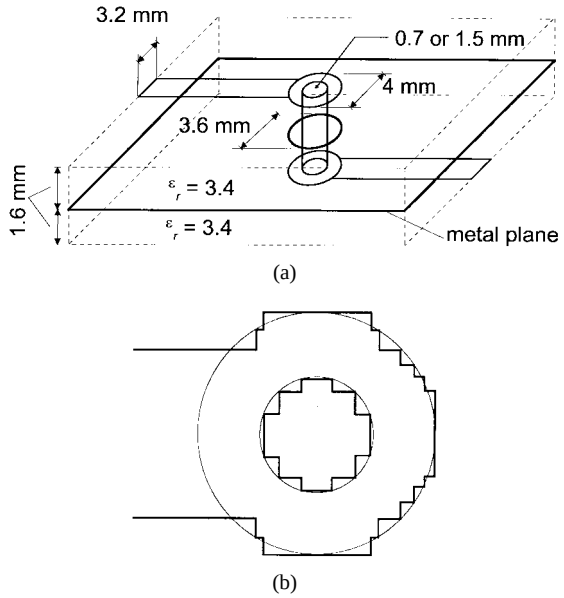

Fig. 2. Model of the via. (a) Geometry. (b) ESN discretization.

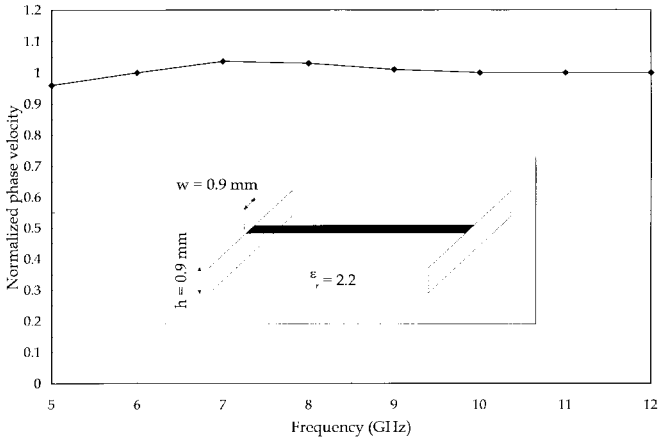

Fig. 3. Normalized phase velocity versus frequency for a uniform microstrip line.

The performance of the proposed PML's was assessed by using three different uniform microstrip transmission lines. One consists of a strip suspended in free space, the second of a strip placed on a grounded substrate with $\varepsilon_r = 2.2$, and the third is identical to the second, but is covered with a superstrate layer of $\varepsilon_r = 10.2$.

The geometrical details of the problem are shown in the inset of Fig. 4. The discretization along x-, y-, and z-axes is uniform with $\Delta = 0.25$ mm and the computational space is subdivided into a $32 \times 32 \times 60$ lattice. The absorption factor is chosen to be $g_{\text{cex}} = g_{\text{cey}} = g_{\text{cmx}} = g_{\text{cmy}} = 0.1$ and the PML wall thickness is 32 cells. The reflections, shown in Fig. 4, are smallest for uniform media ($R = E_{\text{reflected}}/E_{\text{incident}} = 0.9\%$), and increase with the increasing number of dielectric layers. In the case of a single substrate R is 1.9% and increases to 3.1% with the addition of the cover layer.

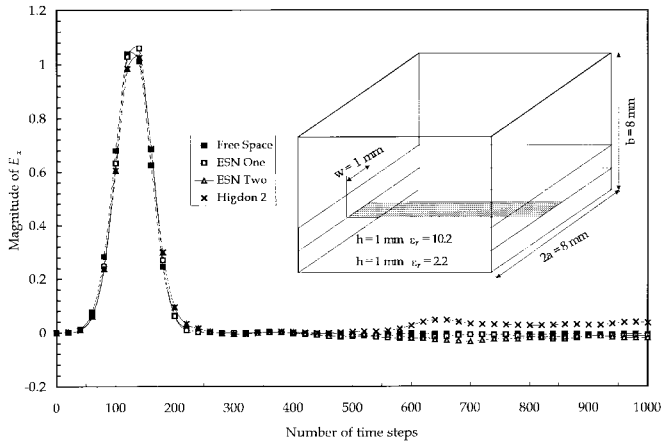

Fig. 4. Reflections of different types of boundary conditions.

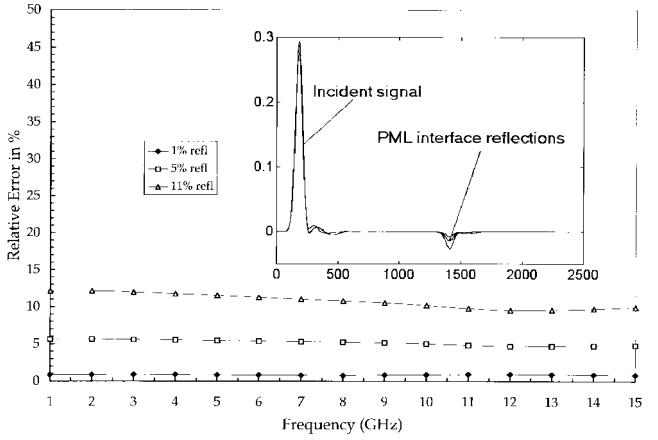

Fig. 5. Frequency-domain errors due to PML artificial reflections.

In order to estimate the influence of the numerical reflections on the S-parameters, the following numerical experiment was carried out. An open microstrip line ($w = 3.2$ mm), suspended at a distance of $h = 1.6$ mm in the air over a ground plane, was chosen for the simulation. It was discretized into a $18 \times 28 \times 200$ lattice ($\Delta = 0.4$ mm), with absorption factors ($g_{\mathrm{cex}} = g_{\mathrm{cey}} = g_{\mathrm{cmx}} = g_{\mathrm{cmy}}$) of 0.15, 0.1, and 0.05, respectively, used to assess the performance of a PML layer composed of 24 cells. The total simulation time was 2400 timesteps, for which the time-domain reflections, shown in the inset of Fig. 5, were 2%, 6%, and 11%, respectively. The error in the frequency-domain, due to the artificial numerical reflections, was computed from the percent error defined as $100 \cdot (V_{\mathrm{TOT}}(f) - V_{\mathrm{incident}}(f))/V_{\mathrm{incident}}(f)$, where V_{TOT} and V_{incident} are Fourier transforms of the total and incident voltage waveforms. When converted to decibels, the same results show that V_{TOT} differs from V_{incident} by 1.1, 0.5, and 0.2 dB, respectively, for the three selected values of the absorption factors.

The frequency response of the via structure, shown in Fig. 2, is given in Figs. 6 and 7 for via diameters of 0.7 and 1.5 mm, respectively. It should be noted that since the discretization of the ESN is based on the rectangular coordinates, the circular shape of the via, pads, and the hole through the ground plane were modeled using a staircase approximation (see Fig. 2).

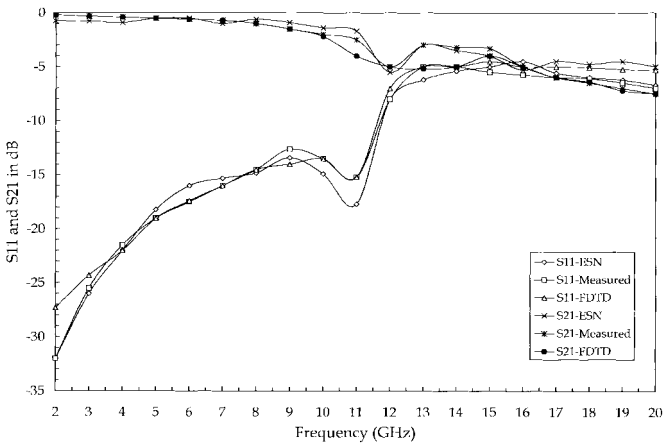

Fig. 6. S_{11} and S_{21} parameters of a through via with the rod diameter of 0.7 mm.

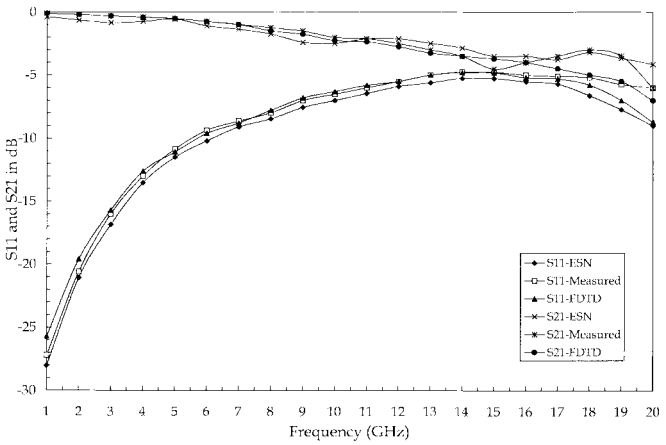

Fig. 7. S_{11} and S_{21} parameters of a through via with the rod diameter of 1.5 mm.

The computed S-parameters of the two vias were compared to measured data and FDTD generated data available in [4]. Note that the agreement between the measured data, the FDTD, and the ESN is very good. The minor discrepancies in the measured and ESN data can be attributed to the differences in the actual geometry and the staircase approximations used in the ESN. On the other hand, the differences between the ESN and FDTD data can be related to different discretization methods—variable and uniform grids used in [4] and ESN, respectively. To generate the data with the ESN, the geometry was uniformly discretized into $32 \times 40 \times 184$ cell lattice ($\Delta = 0.2$ mm).

The numerical computations, based on the ESN, and presented in this paper, were carried out on i486DX2-66 MHz and P5-90 MHz platforms. On the i486DX2-66 MHz platform, the simulation time was 0.16 ms/(cell $\times$ timestep), and 0.056 ms/(cell $\times$ timestep) on the P5. For comparison, the regular SNM implementation of the same problem takes 1.5 ms/(cell $\times$ timestep) on the i486DX2-66 MHz platform and 0.52 ms/(cell $\times$ timestep) on the P5. At the same time, the memory requirements for data storage were significantly different. For the via problem with the lattice of $32 \times 40 \times 184$ cells, approximately 33 Mbytes of memory were required for the

ESN compared to 71.5 Mbytes that would have been necessary to run the SNM.

REFERENCES

[1] K. Wu, M. Yu, and R. Vahldieck, "Rigorous analysis of 3-D planar circuit discontinuities using the space spectral domain approach (SSDA)," *IEEE Trans. Microwave Theory Tech.*, vol. 40, pp. 1475–1483, July 1992.

[2] L. P. B. Katehi and N. G. Alexopoulos, "Frequency dependent characteristics of microstrip discontinuities in millimeter wave integrated circuits," *IEEE Trans. Microwave Theory Tech.*, vol. MTT-33, pp. 1029–1035, Oct. 1985.

[3] H. Jin and R. Vahldieck, "The frequency-domain transmission-line matrix method—A new concept," *IEEE Trans. Microwave Theory Tech.*, vol. 40, pp. 2207–2218, Dec. 1992.

[4] S. Maeda and T. Kashiwa, "Full-wave analysis of propagation characteristics of a through hole using the finite-difference time-domain method," *IEEE Trans. Microwave Theory Tech.*, vol. 39, pp. 2154–2159, Dec. 1991.

[5] N. Yoshida and I. Fukai, "Transient analysis of a stripline having a corner in three-dimensional space," *IEEE Trans. Microwave Theory Tech.*, vol. MTT-32, pp. 491–498, May 1984.

[6] M. Tsai, T. Horng, and N. G. Alexopoulos, "Via hole, bond wire and shorting pin modeling for multi-layered circuits," in *Int. Microwave Symp. Dig.*, vol. 3, 1994, pp. 1777–1780.

[7] J. P. Berenger, "A perfectly matched layer for the absorption of electromagnetic waves," *J. Comp. Phys.*, vol. 114, no. 2, pp. 185–200, Oct. 1994.

[8] D. S. Katz, E. T. Thiele, and A. Taflove, "Validation and extension to three dimensions do the Berenger PML absorbing boundary condition for FDTD meshes," *IEEE Microwave Guided Wave Lett.*, vol. 4, pp. 268–270, Aug. 1994.

[9] A. Bahr, A. Lauer, and I. Wolff, "Application of the PML absorbing boundary condition to the FDTD analysis of microwave circuits," in *Int. Microwave Symp. Dig.*, vol. 1, 1995, pp. 27–30.

[10] J. C. Veihl and R. Mittra, "An efficient implementation of Berenger's perfectly matched layer (PML) for finite-difference time-domain mesh truncation," *IEEE Microwave Guided Wave Lett.*, vol. 6, pp. 94–96, Feb. 1996.

[11] C. Eswarappa and W. Hoefer, "One-way equation absorbing boundary conditions for 3-D TLM analysis of planar and quasi-planar structures," *IEEE Trans. Microwave Theory Tech.*, vol. 42, pp. 1669–1677, Sept. 1994.

[12] L. Zhao and A. Cangellaris, "A general approach for the development of unsplit-field time-domain implementations of perfectly matched layers for FDTD grid truncation," *IEEE Microwave Guided Wave Lett.*, vol. 6, pp. 209–211, May 1996.

[13] C. A. Balanis, *Advanced Engineering Electromagnetics*. New York: Wiley, 1989, pp. 445–449.

Dragos M. Bica (S'94) received the Dipl. Ing. degree in electrical engineering from Politechnica Bucharest, Romania, in 1985, and M.S.E.E. degree from the University of South Carolina, Columbia, in 1994. He is currently working toward the Ph.D. degree in the Department of Electrical and Computer Engineering, University of South Carolina, Columbia.

From 1991 to 1993, he was an Assistant Professor with the Departament Electrotechnica, Politechnica Bucharest. Since 1993, he has been a Research Assistant with the Department of Electrical and Computer Engineering, University of South Carolina. His research interests include computational methods in EM, microwave and digital integrated circuits, signal-integrity analysis, electronic packaging, and computer-software development.

Benjamin Beker (S'83–M'83, SM'94) was born in Vilnius, Lithuania, in 1959. He received the B.S.E.E., M.S.E.E., and Ph.D. degrees from the University of Illinois, Chicago, in 1982, 1984, and 1988, respectively.

From 1982 to 1988 he was a Research Assistant in the Department of Electrical Engineering and Computer Science, University of Illinois, Chicago, working with numerically oriented scattering and radiation problems. In 1988 he joined the Department of Electrical and Computer Engineering, University of South Carolina, Columbia, where he is now an Associate Professor.

His research interests include EM-field interaction with anisotropic materials, computational methods in scattering, radiation, guided-wave propagation in millimeter-wave integrated circuits, and electronic packaging.